Iranian Journal of Chemistry and Chemical Engineering (IJCCE)

Lead removal from aqueous solution by a superior accessible nanoscale zero-valent iron/NaY zeolite adsorbent: Isotherm, kinetic, and thermodynamic studies

Sheikhhassani, Hamed; Ghahremani, Aysan; Manteghian, Mehrdad[1+]; Alinejad-Mir, Ali

Department of Chemical Engineering, Tarbiat Modares University, Tehran, Iran

ABSTARCT: *One of the nowadays' challenges currently confronting the world is the employment of an effective adsorbent on an industrial scale in order to be able to eliminate the heavy metals from the aqueous media. The aim of this study was to assess the effectiveness of a nanoscale zero-valent iron loaded on NaY zeolite (nZVI/NaY zeolite) composite for the sake of removing lead ions. The characteristics of the nZVI/NaY zeolite were determined using XRD, FESEM, and BET analyses. The impact of various parameters, including weight ratio of nZVI to NaY zeolite, pH, adsorbent dosage, contact time, initial concentration and temperature was investigated on adsorption. According to the optimum conditions, which include a pH level of 6, an adsorbent dosage of 0.5 g/L, a contact time of 60 minutes, an initial concentration of 250 mg/L of lead, and an ambient temperature of 25°C, the highest efficiency in the eliminate of lead ions by the nZVI/NaY zeolite composite was 99.25%. The correlation of equilibrium data with Freundlich, Temkin and Langmuir isotherms indicated consistency with Freundlich isotherm. Elovich, Pseudo-first-order, Pseudo-second-order, and Morris-Weber models were used to investigate adsorption kinetics, and nZVI/NaY zeolite showed a good correlation with the Pseudo-second-order. Based on the thermodynamic parameters, it can be inferred that the process of adsorption is feasible, occurs spontaneously, and exothermic. The results demonstrated that the adsorbent had a maximum capacity of 714.3 mg/g. This significant adsorption capacity can be used as an effective parameter on an industrial scale to reduce the lead concentration to an acceptable level. Furthermore, the employed adsorbent is able to be simply separated from the end of the adsorption process via the external magnetic field. These results display that nZVI/NaY zeolite is a superior adsorbent applied to eliminate lead ions from water-based solutions and can be used in water resources recovery and also for the treatment of industrial effluents.*

Key Words*: nanoscale Zero-Valent Iron; Adsorption; NaY zeolite; Lead ions; Isotherm, Kinetic; Thermodynamic*

[1] *To whom correspondence should be addressed.*

[+] *E-mail: manteghi@modares.ac.ir*

INTRODUCTION

Heavy metals are recognized as pervasive environmental pollutants on a global scale. They emanate primarily from industrial effluent and municipal wastewater discharges, posing significant threats to both human health and the environment [1,2]. The detrimental impact of these pollutants has been exacerbated by increased industrialization [3,4].

Moreover, the discharge of untreated wastewater by industries has led to elevated concentrations of heavy metals, including mercury, lead, cadmium, arsenic, and chromium in surface water and groundwater [5,6]. Among these heavy metals, lead stands out as particularly toxic, even at low concentrations, with the potential to accumulate in muscles, bones, and the liver, resulting in severe health issues such as nervous and reproductive system damage, brain damage, anemia, and more [7–9].

Numerous studies have aimed to eliminate heavy metals from industrial wastewater effluent. However, given the high concentrations typically involved, achieving this on an industrial scale is a challenging task [10–12]. Therefore, the quest for practical approaches applicable to industrial-scale wastewater treatment is of paramount importance. Several methods, including ion exchange, membrane separation, chemical precipitation, reverse osmosis, adsorption, solvent extraction, and sedimentation, have been explored for removing these ions from both industrial wastewater and domestic [12,13]. Among these approaches, adsorption has demonstrated exceptional efficiency due to its affordability and simplicity in operation, making it a widely implemented method for heavy metal ion removal [14–16]. Notably, the utilization of synthetic nanoparticles and porous materials, such as zero-valent iron in nanoscale (nZVI), has garnered notable attention [3,17]. Owing to their physico-chemical properties, reduction capacity, and remarkable potential for heavy metal uptake, nZVI emerges as a promising candidate for lead removal from wastewater [18], reducing Pb^{2+} ions to the less reactive Pb^{0} form [19].

However, these nanoparticles come with certain limitations, including low durability, weak mechanical strength, agglomeration tendencies, and susceptibility to oxidation, which may diminish their adsorption effectiveness. To address these challenges, various solutions have been proposed, one of which involves entrapping the nanoparticles within different matrix bases [20,21].

For instance, Zhang et al. [22] investigated the effectiveness of Kaolin-supported nano-scale zero-valent iron (K-nZVI) in adsorbing lead ions from wastewater, observing that K-nZVI efficiently reduced Pb^{2+} to Pb^{0}, even when there are high concentrations of lead heavy metal present.

In another research, Mekkawi et al. [23] synthesized NaY zeolite from various Egyptian kaolins (ZS, ZK, and ZD) and assessed the adsorbents' efficiency in eliminating lead ions from wastewater, reporting a maximum capability of adsorption was 299.6 mg/g.

Besides, utilizing zeolite and Montmorillonite as a base for nZVI (Z-nZVI, Mt-nZVI) has demonstrated notable efficacy in removing lead ions from wastewater. Arancibia-Miranda et al. [24] discovered that Z-nZVI and Mt-nZVI could remove up to 99% of lead ions.

Among the materials suitable for use as a matrix base, synthetic zeolites such as crystalline sodium Y (NaY) zeolites, exhibit great promise. These zeolites are renowned for their high thermal stability, uniform pore distribution, stable framework structure, and nano-sized channels and cages. Their negative surface charge within the neutral pH range imparts excellent cation exchange properties, and their high porosity and cavity volume make

them highly efficient in removing heavy metals from aqueous solutions [25–27]. Notably, there is limited existing literature on the use of NaY zeolites as a support for nZVI in removing heavy metals from aqueous media.

In light of these research gaps, we have selected NaY zeolite as the support for the nZVI/NaY zeolite composite. This innovative adsorbent was synthesized by loading zero-valent iron nanoparticles onto NaY zeolite and evaluated for its efficacy in removing lead ions from wastewater. Characterization of the synthesized adsorbent was achieved through various analyses, including XRD, FESEM, and BET. The study explored the impact of several parameters, including weight ratio, contact time, temperature, adsorbent dosage, initial concentration, and pH on the adsorption process. Furthermore, the experimental results were assessed with the adsorption isotherm, kinetic and thermodynamic approaches to elucidate the adsorption mechanism.

METHODOLOGY

Chemicals

The following materials used in this research were: NaY zeolite (SiO_2/Al_2O_3 = 5.2) from Naike company (China); iron(III) chloride hexahydrate (97%), sodium borohydride (99%), ethanol (96%), lead(II) nitrate salt (99%), hydrochloric acid (37%), and sodium hydroxide (99%) from Merck (Germany). Moreover, deionized water was utilized throughout the tests.

Synthesis of the composite

The preparation of nanoscale zero-valent iron supported on NaY zeolite (nZVI/NaY zeolite) was carried out using the Fe(III) liquid-phase reduction technique, as described elsewhere [28]. To elaborate, 3.5 g of $FeCl_3.6H_2O$ was combined in 100 mL of ethanol-water solution (50 v/v %). This mixture was subsequently poured into a three-necked flask containing 1 gr of NaY zeolite. The components were mechanically stirred under a nitrogen flow for a duration of 10 minutes at room temperature to ensure that there is no presence of air in the reaction environment. After complete mixing, it was transferred to a burette (100ml). Then, a solution comprising $NaBH_4$ (2.5 g of $NaBH_4$ dissolved in 100 mL of deionized water) was slowly dripped onto the stirring mixture in a three-necked flask containing NaY zeolite and iron salt in a nitrogen atmosphere. This action corresponds to the reduction reaction declared in Equation (1). After adding the $NaBH_4$ solution, the mixture was stirred for another 30 minutes, while maintaining a nitrogen atmosphere. The resultant murky solid was isolated through vacuum filtration, employing a Buchner funnel and Whatman filter paper of grade No. 1. The solid was rinsed three times using 25 mL of ethanol each time, and subsequently dehydrated in vacuum dryer at 70°C for ten hours. It should be mentioned that a similar approach was employed to produce nZVI, but without using NaY zeolite [28,29].

$$4Fe^{3+} + 3BH_4^- + 9H_2O \rightarrow 4Fe^0_{(s)} \downarrow + 3B(OH)_3 + 9H^+ + 6H_{2(g)} \quad (1)$$

Characterization

Several methods and tools were utilized to assess the characteristics of the produced composite. Technical abbreviations such as XRD were explained when initially used. Additionally, correct British spellings, grammar, and conventions were applied consistently throughout the revised version. A PHILIPS PW 1730 instrument with CuK α radiation was used to conduct X-ray diffraction (XRD) analysis in the range of 2θ from 10 to 80 degrees, with a wavelength of γ=0.154056 nm, voltage of 40 kV, and current of 30 mA. This facilitated the identification of the crystal structure and compounds present in the samples. The text was written in a formal and objective manner, avoiding any bias, slang, subjective language, and filler words. The morphology and dimensions of

nanoparticles were investigated using a TESCAN/MIRA3 instrument by taking field emission scanning electron microscopy (FESEM) images at different magnifications. Before the imaging process, the sample surfaces were coated with sputtered gold to enhance conductivity and image quality. The utilization of this procedure provides valuable insight into the characteristics of the nanoparticles. The Brunauer-Emmett-Teller (BET: BELSORP MINI II) technique was employed to ascertain, mean diameter of the samples, pore volume and the specific surface area. This involved measuring the quantity of nitrogen gas that was adsorbed and released by the substance under a constant temperature of liquid nitrogen (-196°C). During the BET analysis, the specimen was submerged in a container filled with liquid nitrogen. The quantity of gas adsorbed by the material was determined by successively augmenting the nitrogen gas pressure at each stage while the desorption rate was evaluated by steadily reducing the gas pressure. The quantity of gas adsorbed by the material was determined by successively augmenting the nitrogen gas pressure at each stage while the desorption rate was evaluated by steadily reducing the gas pressure. Additionally, a Shimadzu AAS: AA-670 spectrophotometer was employed to ascertain the concentration of lead.

Batch experiments

A series of batch tests were conducted to explore the impact of distinct adsorption factors, including weight ratio, pH, adsorbent dosage, contact time, initial concentration and temperature, and to ascertain the optimal values for accomplishing the highest possible removal of lead. The trials were conducted in 100 mL glass containers with 50 mL of lead solution at various concentrations. To examine the weight ratio in the composite, we prepared adsorbents using various weight proportions of 1: 1, 1: 2, 1: 4 and 1: 8 nZVI to NaY zeolite. Subsequently, we determined optimum adsorbent. We evaluated the effect of pH in the pH range of 3 to 8 by conducting experiments. The pH of the mixture was regulated through 0.1 M NaOH and HCl solutions. We determined the time required to achieve equilibrium using various time intervals ranging from 3 to 180 minutes. The adsorbent dosages were varied between 0.25, 0.5 and 1 g/L in the conducted experiments. Additionally, the influence of initial lead concentration and temperature on the process of adsorption was examined. The lead concentration was varied from 50 to 1000 mg/L, and the temperature was adjusted between 25 to 55 °C to determine the impact on adsorption quantity. Technical term abbreviations were defined when initially used to enhance clarity. The impact of these variables was examined to ensure objective analysis. An atomic adsorption spectrometer was employed to measure the residual concentration of lead in the solution, and constant stirring was maintained at a speed of 300 rpm for the length of the experiments. After analyzing the results obtained for varying initial concentrations and temperatures, we optimized all parameters to determine the adsorbent's optimal performance in the most efficient water treatment scenario [30].

In all conducted experiments, the removal efficiency (R %) and the quantity of adsorbed ions per unit mass of adsorbent were determined using Eq. (2) and Eq. (3):

$$R\% = \frac{C_i - C_f}{C_i} \times 100 \quad (2)$$

$$q = (C_i - C_f) \times \frac{V}{M} \quad (3)$$

C_i and C_f denote initial and final concentrations of adsorbed lead metal (mg/L), correspondingly, V indicates the lead solution volume (L), and M stands for the mass of the adsorbent (g) [31,32].

Isotherm and kinetic studies

To ascertain the lead adsorption capacity of the nZVI/NaY zeolite composite, equilibrium isotherms models can be utilized. Equilibrium data matching with isotherms can also be employed to determine the optimal adsorption isotherm and minimize adsorbent consumption. The adsorption mechanism can be defined using adsorption isotherm constants to determine surface properties and adsorption correlation, thus providing physicochemical data [25,33].

Therefore, in this research, Langmuir, Freundlich, and Temkin equilibrium adsorption isotherms were utilized, whose equations are summarized along with their parameters in Table1.

Table 1: The equations of equilibrium isotherm models [34]

Isotherms	Equations	Parameters
Langmuir	$\frac{1}{q_e} = \frac{1}{K_L q_{max} C_e} + \frac{1}{q_{max}}$ (4)	K_L, q_{max}
Freundlich	$\ln(q_e) = \ln(K_F) + \frac{1}{n}\ln(C_e)$ (5)	K_F, n
Temkin	$q_e = B\ln(A) + B\ln(C_e)$ (6)	A, B

According to Table1, in the Langmuir isotherm, q_e (mg/g) is the equilibrium adsorption capacity, C_e (mg/L) is the equilibrium concentration, q_{max} (mg/g) is the maximum adsorption capacity, and K_L (L/mg) is Langmuir adsorption constant. It is noteworthy that K_L constant is proportional to the adsorption energy and enthalpy change (Eq. (4)).

In the Freundlich isotherm, $K_f(\frac{mg^{1-1/n}L^{1/n}}{g})$ and n are Freundlich and heterogeneity coefficients corresponding to adsorption capacity and intensity or surface heterogeneity, respectively (Eq. (5)) [35]. Also, B is Temkin constant corresponding to the adsorption heat (J/mol), and A is Temkin equilibrium binding constant (L/g) (Eq. (6)) [34,36].

The study utilized pseudo-first-order, pseudo-second-order, Elovich, and Morris Weber equations to determine the kinetics of adsorption. The efficiency of adsorption is largely dependent on its kinetics. Table 2 presents the different kinetic models and their respective parameters [37,38].

The adsorption operation is controlled by the chemical reaction in the models of pseudo-first-order, pseudo-second-order, and Elovich. The Elovich model describes adsorption on the adsorbent surface in such a way that the desorption of adsorbate is not possible, making it suitable for chemical adsorption processes (Eq. (9)). The Morris Weber model emphasizes the critical role played by intraparticle diffusion in controlling the adsorption process (Eq. (10)).

Table 2: The equations of kinetic models [39]

Kinetic model	Equations	Parameters
pseudo-first-order	$\log(q_e - q_t) = \log(q_e) - \frac{k_1 t}{2.303}$ (7)	q_e, k_1
pseudo-second-order	$\frac{t}{q_t} = \frac{1}{k_2 q_e^2} + \frac{t}{q_e}$ (8)	q_e, k_2
Elovich	$\frac{dq_t}{dt} = \alpha \exp(-\beta q_t)$ (9)	α, β
Morris Weber	$q_t = K_{id} t^{0.5} + C$ (10)	K_{id}, C

The kinetic constants in table 2 are as follows: k_1 (1/min) is the first-order rate constant, k_2 (g/mg.min) is second-order rate constant, and k_{id} (mg/g.min$^{0.5}$) is intraparticle intensity constant. The Equilibrium adsorption capacity and the adsorption capacity at time t are q_e (mg/g) and q_t (mg/g), respectively. Also, C (mg/g) refers to thickness of the boundary layer. The initial adsorption and desorption rate constants are α and β in the Elovich kinetic model, correspondingly [40–42].

RESULT & DISCUSSION

Characterization

XRD analysis

The XRD patterns of nZVI and NaY zeolite functionalized with nZVI (nZVI/NaY zeolite) were illustrated in Figure 1. When first used, technical terms are clearly explained, and concise, simple sentences enhance clarity and flow. The observed pattern indicates that the reaction conditions likely affected the synthesis of zero-valent nanoparticles, resulting in an amorphous structure (Fig. 1(a)). Also, the language used is value-neutral, free from bias, and avoids filler words and unnecessary jargon. It is evident that the pattern of nZVI shows a single peak at 2θ=45°, indicating the presence of Fe^0. Standard language and formal tone contribute to objectivity while adhering to British English spelling and grammatical correctness. There are no iron oxide peaks present in this pattern [24,43], indicating successful prevention of oxidation of the nanoparticles during the synthesis process. Additionally, the pattern of the nZVI/NaY zeolite composite displays an amorphous structure. The peaks at 2θ = 15.8°, 20.5°, 27.1° and 31.4° (Figure 2(a)) indicate the existence of NaY zeolite, consistent with the previous literature [44,45]. Besides, the crystal planes (3 3 1), (4 4 0), (6 4 2), and (7 5 1) are related to NaY zeolite, and the crystal plane (1 1 0) is corresponded to nZVI, that reported from literature and, agreed to the peaks observed in the XRD pattern for nZVI/NaY zeolite composite [46,47].

The standard diffraction peak of zero-valent iron nanoparticles at 2θ = 45° reveals that the NaY zeolite support underwent functionalization with nanoparticles, despite the diminished intensity [48]. This is explicable by the fact that the attenuation in zero-valent iron intensity is attributed to the existence of the NaY zeolite, which contains a diverse range of compounds, such as alumino silicates. The occurrence of zero-valent iron peaks within the modified adsorbent pattern demonstrates that the nanoparticles were precisely positioned within the zeolite matrix, as noted in reference [25].

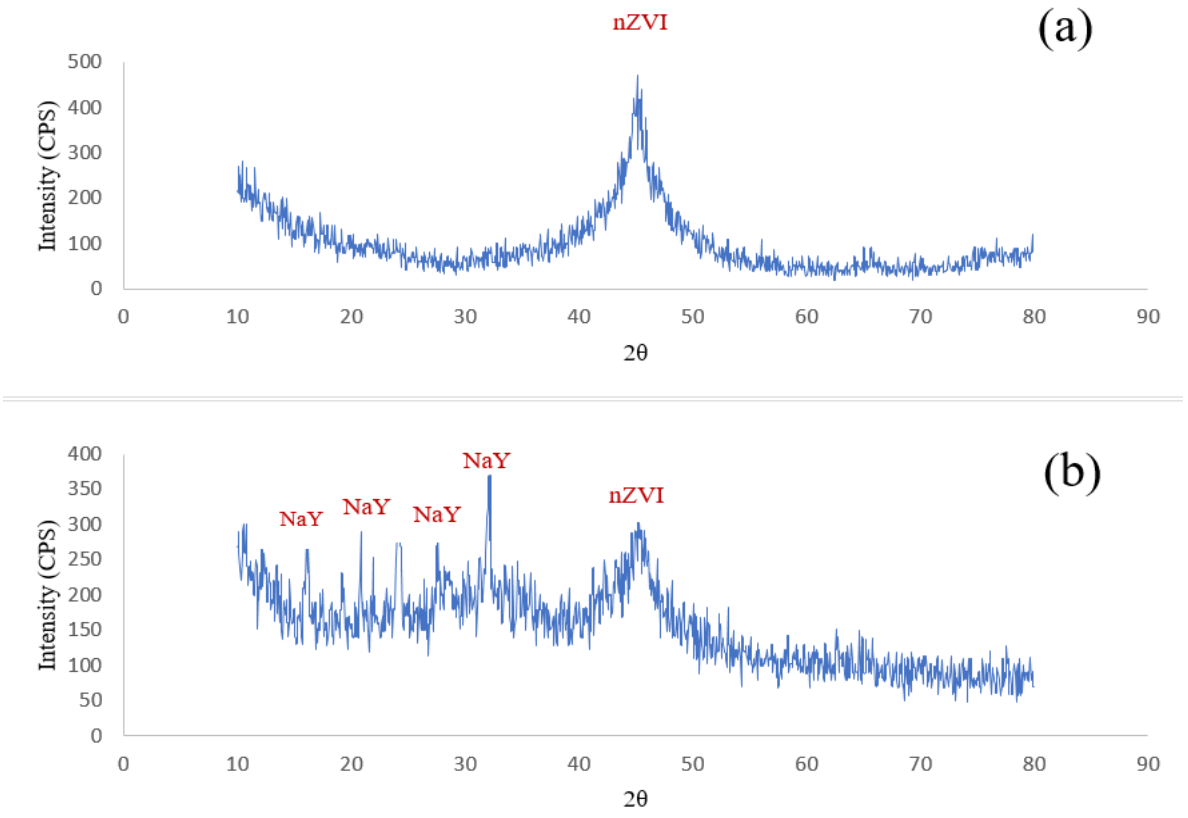

Fig. 1: XRD patterns of adsorbents (a) nZVI, and (b) nZVI/NaY zeolite composite

FESEM analysis

The surface morphology of NaY zeolite and nZVI/NaY zeolite composite was determined using a FESEM analysis. Figure 2(a) illustrates that the NaY zeolite possesses a smooth crystalline structure without any surface roughness. FESEM results demonstrate that the particle size of NaY is less than 1 micron. Upon modification of NaY zeolite with zero-valent iron nanoparticles, the adsorbent surface becomes roughened, thereby confirming the location of nanoparticles on the adsorbent, as depicted in Figure 2(b). Although NaY zeolite was utilized as a support to prevent nanoparticle aggregation, the images indicate that magnetic forces cause some nanoparticle adherence. A significantly reduced degree of aggregation was observed amongst these nanoparticles, as previously reported in studies [49,50]. This suggests that decreasing the loading ratio provides more space for nanoparticles to be distributed uniformly and regularly on the surface of NaY zeolite. This could potentially enhance the adsorbent's effectiveness. Furthermore, the synthesized nanoparticles display a diameter of approximately 10 to 65 nanometers, indicating the nanometric synthesis of zero-valent iron [51,52]. As a result, when combined with NaY zeolite as a supporting material, nZVI creates a superior composite that improves the adsorption process's efficiency.

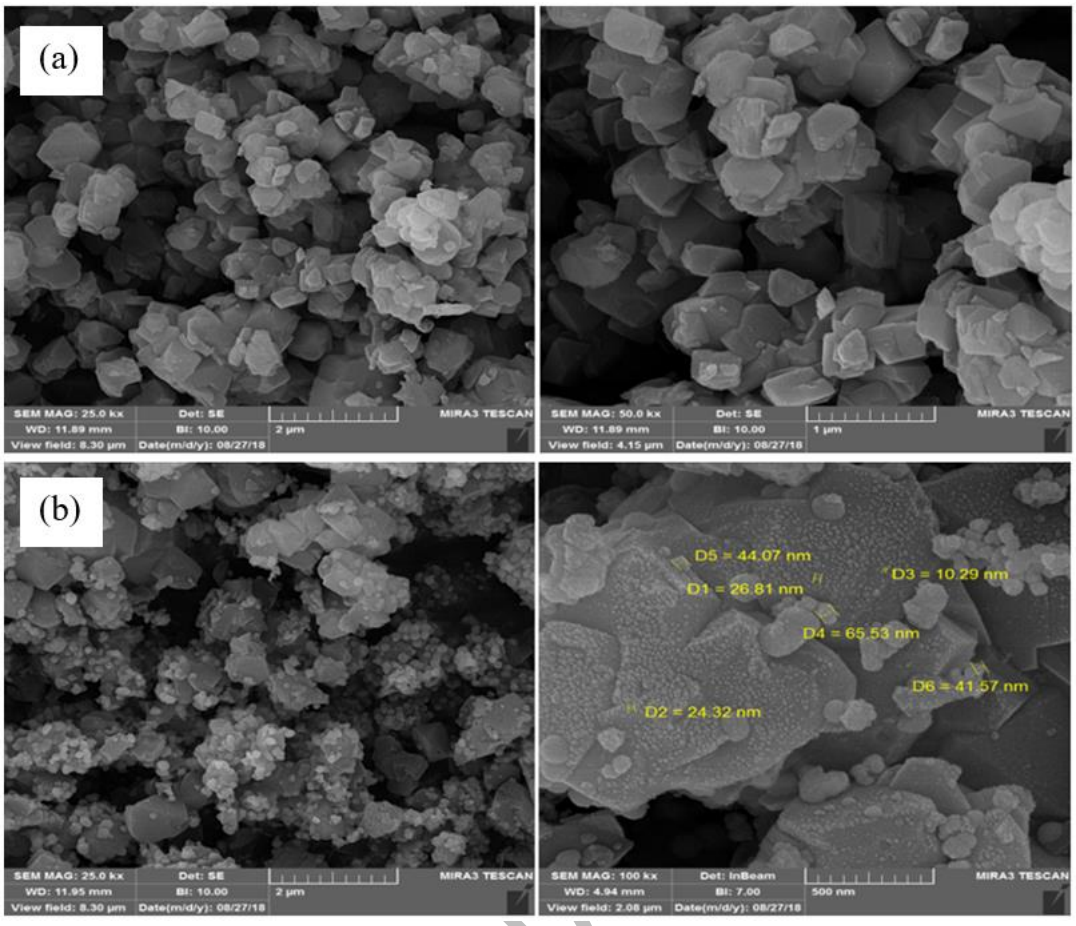

Fig. 2: FESEM images of adsorbents (a) NaY zeolite, and (b) nZVI/NaY zeolite composite

BET analysis

Figures 3 and 4 present nitrogen adsorption-desorption isotherm curves for nZVI and nZVI/NaY composite zeolites. Table 3 displays mean pore diameter, specific surface area, and total pore volume. As per the IUPAC classification, nZVI is a type (IV) material linked to mesopore materials (Fig. 3(a)) [45,53]. Moreover, nZVI/NaY zeolite is expectedly of type (I) and (IV), linked to microporous and mesoporous materials. The shape of the isotherm may be influenced by the composite character. Type (I) is associated with the NaY zeolite according to previous research, and this can cause a slight alteration in the shape of the composite isotherm (Fig. 3(b)). Within the pressure range of 0.3-0.95, the adsorbents show an H_3/type hysteresis loop attributed to capillary condensation [45]. A break point is observed at the onset of the curve in which the initial layer is absorbed entirely, and the subsequent layers commence filling (Fig. 3(b)).

The data in Table 3 shows that the nZVI and nZVI/NaY zeolite composite have specific surface areas of 21.17 m^2/g and 418.6 m^2/g, pore volumes of 0.3501 cm^3/g and 0.2604 cm^3/g, and mean pore diameters of 4.96 nm and 3.34 nm, respectively. It is significant to note that both adsorbents have been classified as mesoporous since the average pore diameter ranges from 2 to 50 nm [54–56].

Moreover, Figure 4 demonstrates the pore size distribution of both nZVI and nZVI/NaY zeolite composite, which confirms their mesoporous nature. The literature reports that the NaY zeolite employed in this research had an approximate specific surface area of 625 m^2/g. Table 3 shows that the specific surface area of NaY zeolite was reduced to 418.6 m^2/g following correction with zero-valent iron nanoparticles [51,57,58]. The decrease is attributed to the positioning of low surface area nanoparticles on the NaY zeolite and their subsequent filling of the pores. It is evident that reducing the weight proportion of nanoparticles to NaY zeolite can enhance the modified adsorbent's specific surface area, thus achieving more effective heavy metal removal by the composite.

Upon analysis of the data regarding lead removal using the modified adsorbent, it was discovered that, despite a reduction in specific surface area, the overall efficiency of the modified adsorbent surpassed that of the original sample. This observation serves to highlight how factors other than specific surface area play an essential role in the process of adsorption and can compensate for its apparent drawbacks. The modified adsorbent can reduce Pb^{2+} ions to a less active form of Pb^0, indicating its ability. Furthermore, the nZVI/NaY zeolite composite displays a desirable specific surface area, making it an appropriate adsorbent for eliminating heavy metals and treating polluted water [59,60].

Table 3: BET analysis of nZVI and nZVI/NaY zeolite composite

Sample	**Surface area (m^2/g)**	**Mean pore diameter (nm)**	**Pore volume (cm^3/g)**
nZVI	21.17	4.96	0.3501
nZVI/NaY zeolite composite	418.6	3.34	0.2604

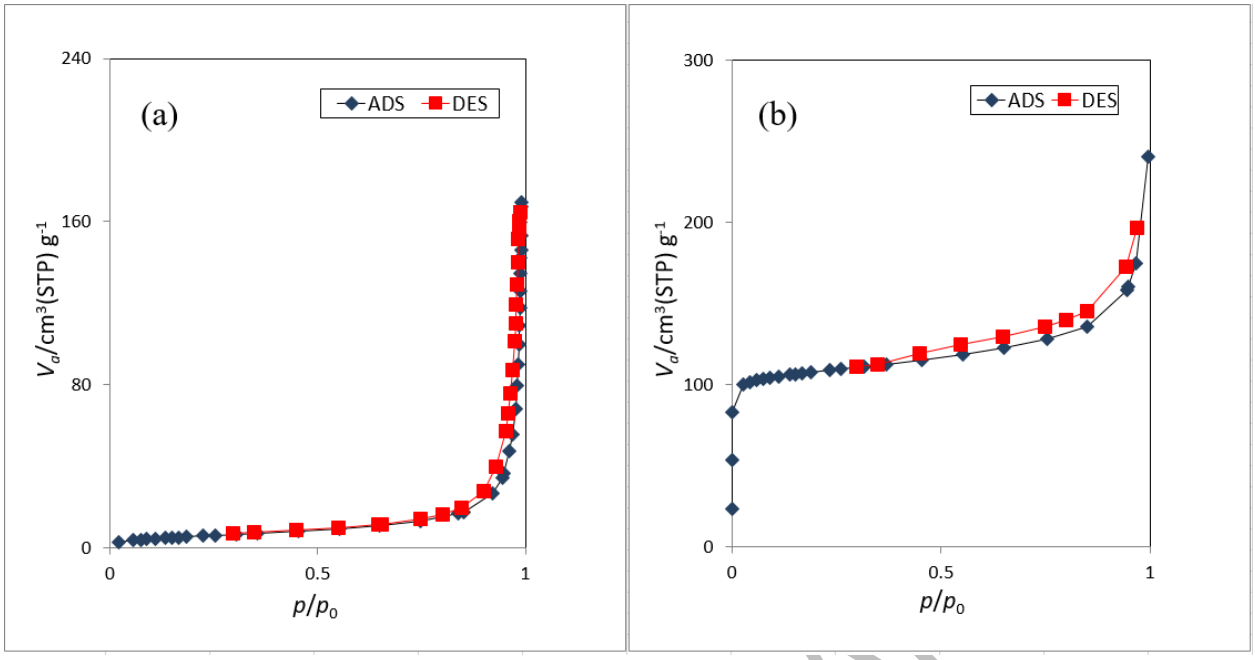

Fig.3: N_2 ***Adsorption-desorption isotherms of adsorbents (a) nZVI and, (b) nZVI/NaY zeolite composite***

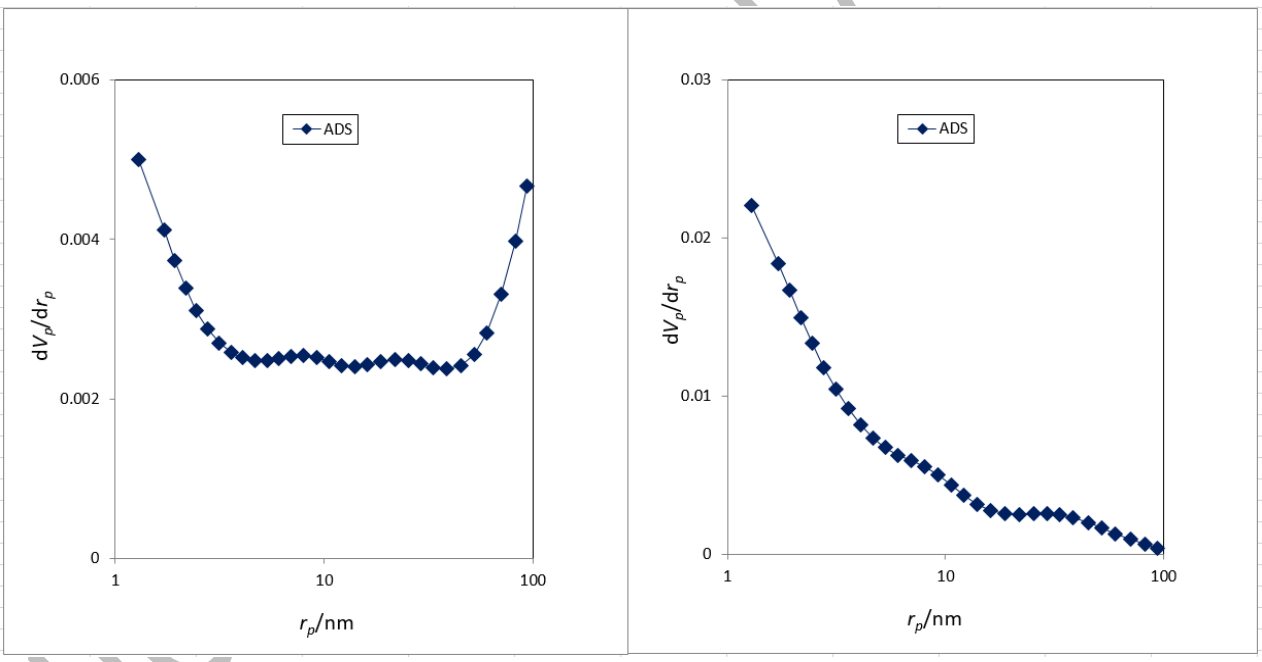

Fig.4: Pore size distribution of adsorbents (a) nZVI and, (b) nZVI/NaY zeolite composite

Removal of Pb^{2+} from aqueous solution

Determination of optimum adsorbent

Adsorbents containing weight ratios of 1:1, 1:2, 1:4, and 1:8 nZVI to NaY zeolite were synthesized to examine how the weight ratio influences the lead ions removal from aqueous solutions. To allow for better comparison of results, nZVI and pure NaY zeolite were tested under identical conditions (pH=6, adsorbent dosage=0.5 g/L, initial lead concentration=250 mg/L, contact time=60 minutes, and ambient temperature). Figure 5 illustrates the impact of weight ratios of nZVI to NaY zeolite on the removal effectiveness. It is evident that the absence of NaY zeolite

resulted in inferior performance of nZVI compared to other synthesized adsorbents, due to agglomeration and a significant drop in the nanoparticles' specific surface area. Similar findings were reported in previous studies [24,28].

By modifying NaY zeolite with nZVI, the effectiveness of eliminating lead ions from the aqueous solution increases up to a weight ratio of 1:4 nZVI/NaY zeolite and subsequently decreases. At ratios of 1:1 and 1:2, the high percentage of nanoparticles to NaY zeolite reduces the available surface area of the nanoparticles for organized and uniform dispersion, leading to their dense packing together. The aggregation hinders the nanoparticles' effectiveness in converting Pb^{2+} ions to Pb^{0}. Additionally, when using a 1:8 nanoparticle to NaY zeolite ratio, excessive reduction in the zeolite's nanoparticles rate greatly diminishes the number of zero-valent iron nanoparticles that can remove Pb^{2+} concentration. As per the outcomes, the proportion of 1:4 of zero-valent iron nanoparticles and NaY zeolite was identified as the most effective and efficient synthesized adsorbent, achieving a 99.25% removal efficacy [18,28].

The enhanced adsorption efficiency of the composite for lead ions removal from aqueous media is because of the synergistic effect of nZVI and NaY zeolite. Moreover, the distinctive nanoscale characteristics and magnetic nature of nZVI can improve the supporting properties of NaY zeolite, thus increasing the removal efficiency. While the augmented lead removal efficiency of the synthesized composite is modest, its favorable outcomes encompass enhanced properties of nZVI and NaY zeolite, lessened nanoparticle usage, and simplified adsorbent separation via the external magnetic field, prevention of nanoparticle agglomeration, substantial growth in adsorption capacity and the creation of a pioneering composite.

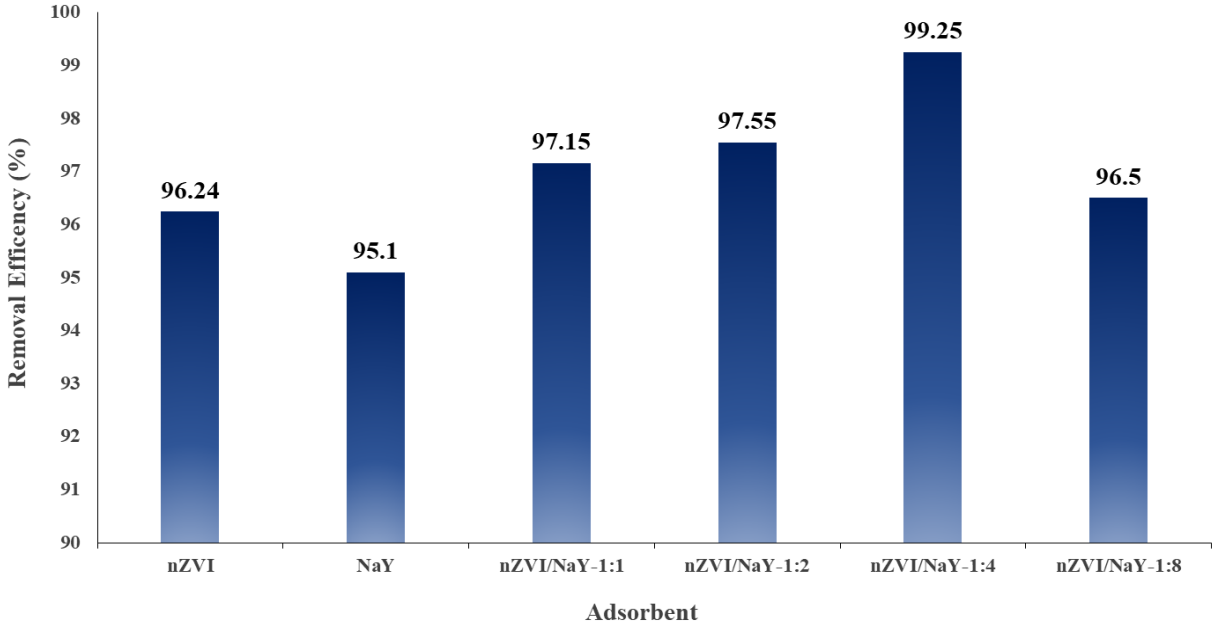

Fig. 5: Effect of weight ratios nZVI to NaY zeolite on the removal efficiency of lead ions from aqueous solution

Effect of pH

The adsorbent's surface charge, the degree of ionization, and the speciation of the adsorbate during the process of adsorption significantly affect the decrease in lead heavy metal concentration in an aqueous solution based on pH. During pH range of 3 to 8, the pH effect on the adsorption of lead was assessed through nZVI/NaY zeolite composite, and the findings are illustrated in Figure 6. The tests were carried out under specific circumstance including an initial concentration of 250 mg/L, adsorbent dosage of 0.5 g/L, contact time of 60 minutes, and ambient temperature. Based on the obtained findings, lead ions transform their nature and shape lead hydroxide [15,19], which precipitates in the water solution at pH = 7. Therefore, pH values higher than pH=8 were not analyzed due to their limited significance.

The experiment indicates that as the solution pH rises to 6, the removal efficiency of lead ions rises and reaches 99.25% at pH=6. However, the efficiency of removal decreases as the pH level rises. The results were examined by scrutinizing the charge on the surface of the synthesized composite and the presence of H^+ ions competing with metal cations in solution. Studies indicate that in the acidic and neutral pH range, the surface charge of nZVI is positive, while the charge on the surface of NaY zeolite is positive at a pH less than 2 and negative at a pH greater than 2 [6,24]. It is worth noting that technical terminologies are explained when first used, and the writing adheres to conventional academic structure, clear language, and precise word choice.

Upon the entrapment of nZVI in the NaY zeolite matrix lattice, the synthesized adsorbent acquires a negative surface charge within the neutral pH range. This negation of the adsorbent surface charge at neutral pH increases the removal efficiency of the synthesized adsorbent. An examination of the trend displayed in Fig. 6 shows that

maximum removal efficiency is achieved at neutral pH. At low pH levels, the efficiency of removal decreases due to the high concentration of H^+ ions in the water solution. These ions compete with the metal cations for binding to the matrix lattice. When the pH level rises, the concentration of H^+ ions reduces, facilitating the deposition of lead ions on the adsorbent surface. However, at a pH of 8, the removal performance reduces as a result of the conversion of lead ions into the hydroxide form. Notably, similar observations are documented in other research studies [24,61].

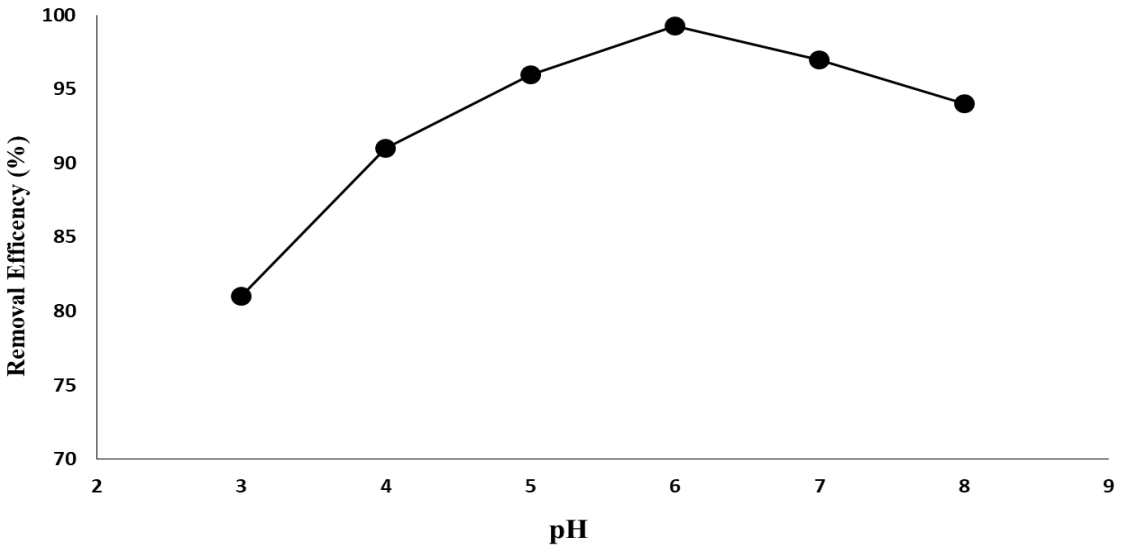

Fig. 6. The Effect of pH on the removal efficiency of lead ions by nZVI/NaY zeolite composite from aqueous solution

Adsorption kinetic studies

The study aims to examine the adsorption process kinetics via contact time and adsorbent dosage. Experimental procedures undertook adsorbent dosages of 0.25, 0.5 and 1 g/L with intervals spanning 3 to 180 minutes. The analyses were conducted at pH=6 and an initial concentration of 250 mg/L and ambient temperature. Figure 7 presents the results obtained. It is evident that the elimination rate of lead ions rose from 84.5% to 99.25% as the adsorbent quantity was increased from 0.25 to 0.5 g/L. On increasing the adsorbent dosage to 1 g/L, the adsorption efficiency is roughly at 99.8%. In reality, the escalation of the adsorbent dosage heightens the accessibility of active sites for lead ions, thus boosting the adsorption efficiency. Conversely, when the quantity of adsorbent is augmented, the availability to high energy active sites is diminished, and the amount of low energy active sites rises. This reduction in active sites results in a decrease in adsorption capacity, as stated in [6,62].

Based on the findings, there was no significant change in removal efficiency when the adsorbent dosage was increased from 0.5 to 1 g/L. In addition, the adsorption efficiency was more than 98% at 0.5 g/L, making it the optimal dosage for the synthesized composite. The adsorption capacity is another critical parameter that effectively determines the adsorbent dosage. When the adsorbent dose is 0.5 g/L, the capacity for adsorption

equals 496.25 mg/g. However, selecting a dose of 1 g/L reduces the adsorption capacity to 249.5 mg/g. It is noteworthy that the synthesized composite, employed as lead ion adsorbent in water media, shows one of the best adsorption capacities in comparison to other studies, considering the amount used [63]. Additionally, contact time was examined as another parameter. In most cases, the adsorption process occurred within the first 30 minutes for all adsorbent doses, reaching equilibrium after 60 minutes. The utilization of nZVI to alter NaY zeolite was the primary cause for the swift adsorption of lead-heavy metals from aqueous media. The synthesized nZVI, owing to its nanoscale, possesses high chemical activity and promptly converts Pb^{2+} ions in aqueous solution into the Pb^{0} form. The rapid elimination of lead ions from the aqueous solution is achieved due to the high reduction rate. The high surface to volume ratio of the nanoparticles results in their increased chemical activity, which is the main contributing factor. This trend has also been observed in other experiments using nZVI to remove heavy metals from aqueous media [61].

The adsorption kinetics were evaluated by fitting the experimental outcomes with the pseudo-first order, pseudo-second order, Elovich, and Morris Weber kinetic models using distinct adsorbent dosages. The corresponding results are illustrated in Table 4. It can be observed that the majority of the removal transpires within the first 30 minutes of the adsorption procedure. Based on the correlation coefficients of the Morris Weber model combined with the laboratory data fitting outcomes, it is apparent that the connected plots are non-linear. Thus, the intraparticle model does not govern the adsorption process, and other mechanisms govern the kinetics of adsorption [40]. Upon reviewing the findings presented in Table 4, it is evident that the correlation coefficient is consistent with the pseudo-second-order kinetic model. Therefore, it can be concluded that the kinetic data align perfectly with this model (R^2=0.999). The laboratory data correlates with the pseudo-second-order model, illustrating that chemical sorption or ion exchange between the adsorbate and adsorbent primarily governs the removal rate of the adsorption process [64].

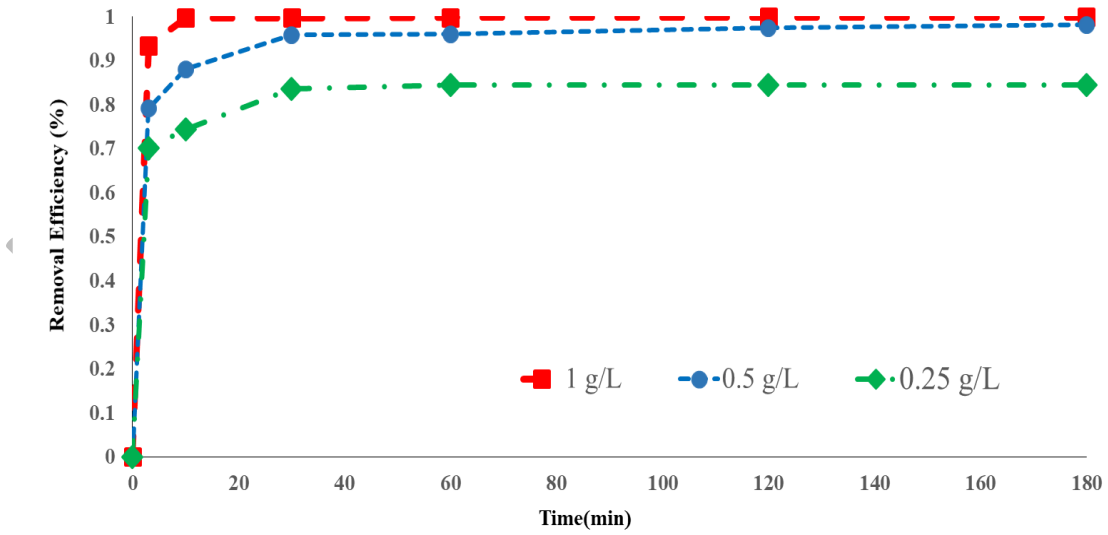

Fig. 7: The effect of contact time on the removal efficiency of lead ions using nZVI/NaY. The experiment was performed at various adsorbent dosages.

Eventually, to determine the kinetic equation controlling the adsorption and a more detailed investigation, the normalized standard deviation (Δq_e) for the pseudo-1st-order and pseudo-2nd-order models was calculated (Eq. (11)).

$$\Delta q_e(\%) = 100\sqrt{\frac{\sum(\frac{q_{e,exp}-q_e}{q_{e,exp}})^2}{N}} \quad (11)$$

Where q_e, exp represents the experimental adsorption capacity and q_e indicates the adsorption capacity once equilibrium conditions have been reached. N represents the number of measurements taken. Notably, a smaller calculated normalized standard deviation indicates that the kinetic model aligns more closely with the experimental data. According to Table 4, the normalized standard deviation value is reduced for the pseudo-second-order kinetic equation, signifying that a strong concurrence exists between this model and experimental outcomes [65].

Table. 4: Kinetic parameters for the removal efficiency of lead ions nZVI/NaY zeolite composite from aqueous solution

Model; adsorbent dose (g/L)	**Parameters**				
Pseudo-first-order	q_e (mg/g)	k_1	q_e, exp (mg/g)	R^2	Normalized Standard Deviation Δq_e%
0.25	616.59	0.069	845	0.910	53.601
0.5	218.77	0.086	497.5	0.941	
1	77.62	0.088	249.75	0.775	
Pseudo-second-order	q_e (mg/g)	k_2	q_e, exp (mg/g)	R^2	
0.25	854.7	1.462	845	0.999	3.408
0.5	526.31	0.95	497.5	0.999	
1	250	10	249.75	0.999	
Elovich	α	β		R^2	
0.25	$14.28 * 10^8$	0.026		0.872	
0.5	$64.37 * 10^6$	0.038		0.921	
1	$33.91 * 10^{56}$	0.54		0.885	
Morris Weber	k_{id}	C		R^2	
0.25	11.59	720.36		0.674	
0.5	7.81	412.16		0.720	
1	0.55	243.74		0.686	

Adsorption isotherms studies

The impact of initial concentration of lead ions on the efficiency of adsorption was defined using the experimental data, and the data was fitted with equilibrium isotherms. The adsorption experiments were conducted under the following conditions: pH=6, adsorbent dosage =0.5 g/L, contact time=60 minutes, and room temperature. The obtained results are presented in Fig. 8. It is evident that the adsorption efficiency reduces as the initial concentration of lead in the aqueous solution rises, with 78.5% achieved at an initial concentration of 1000 mg/L. The leading cause of this decline is the active sites on the synthesized composite surface reacting efficiently with the lead ions when the initial concentration is low. Conversely, the active sites on the adsorbent surface become inadequate as the initial concentration of lead ions increases and cannot interact adequately with the metal ions. Although the adsorbent cannot fully adsorb the metal ions, there is a clear upward trend in changes in adsorption capacity. Figure 9 illustrates how, as the initial concentration increased, the adsorption capacity rose from 99.9 mg/g to 1652 mg/g at initial concentrations of 50 mg/L and 1000 mg/L, respectively. Table 5 contains the fitting results of Freundlich, Temkin, and Langmuir isotherms with the experimental equilibrium data. From the results obtained, the Freundlich isotherm exhibited the highest correlation coefficient, with experimental equilibrium data exhibiting the most consistency to this isotherm (R^2=0.985). The heterogeneity of the adsorbent surface is illustrated by this case, indicating non-uniform distribution of active sites across its surface. The adsorbent surface contains adsorption centers with varying slopes. The most stable sites are filled first, followed by the remaining adsorption centers based on their strength [28,62,66]. Additionally, the maximum adsorption capacity for nZVI/NaY is 714.28 mg/g based on the Langmuir isotherm parameters.

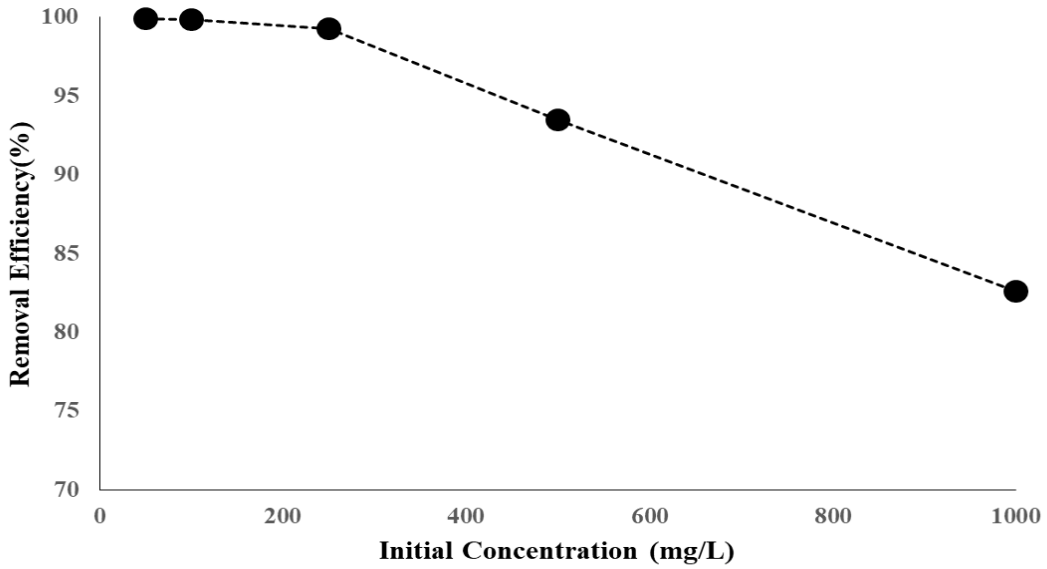

Fig. 8: The Effect of initial concentration on the removal efficiency of lead ions by nZVI/NaY zeolite composite from aqueous solution

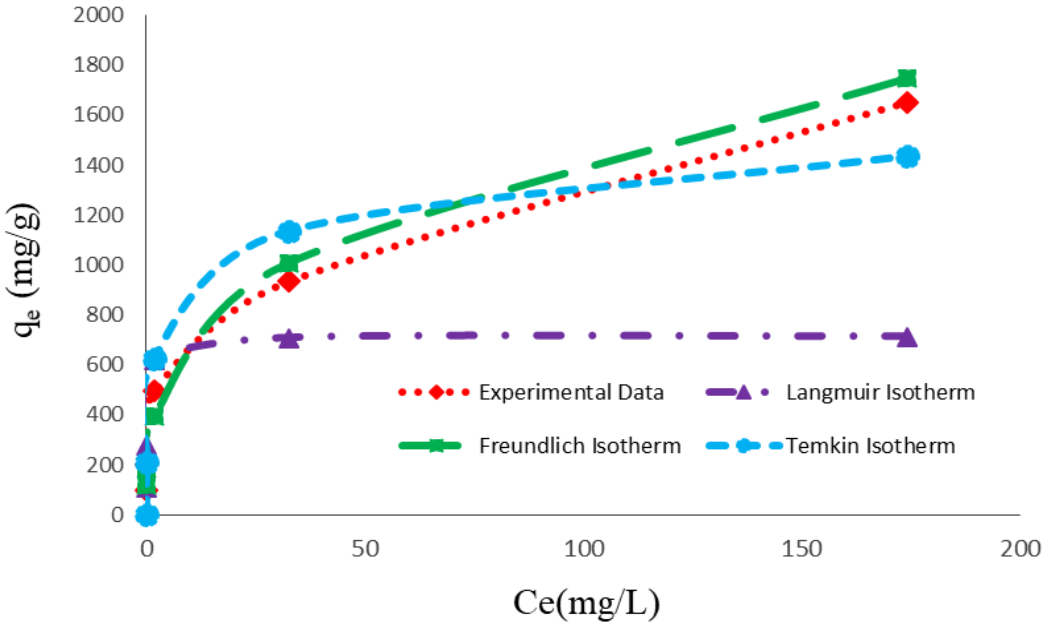

Fig. 9: Various isotherms for lead ions adsorption by nZVI/NaY zeolite composite from aqueous solution

Table. 5: Different Parameters of equilibrium isotherms for the lead ions adsorption by nZVI/NaY zeolite composite from aqueous solution

Langmuir isotherm			Freundlich isotherm			Temkin isotherm		
$\mathbf{q_{max}}$ $(\frac{\mathbf{mg}}{\mathbf{g}})$	K_L $(\frac{L}{mg})$	R^2	K_f $(\frac{mg^{1-1/n}L^{1/n}}{g})$	n	R^2	A	B	R^2
714.28	3.50	0.962	321.17	3.04	0.985	17.81	178.38	0.926

Adsorption thermodynamics

Thermodynamic interpretations of adsorption, when positioned with kinetic models and equilibrium isotherms, can provide clarity on the removal mechanism of heavy metals [67]. The effect of temperature on adsorption efficiency was studied at temperatures ranging from 25 to 55 °C. All experiments were conducted under specific conditions (pH=6, adsorbent dosage=0.5 g/L, initial concentration=250 mg/L and contact time=60 minutes) and the outcomes are illustrated in Figure 10. It is evident that as the temperature increased, the elimination rate dropped from 99.25% at 25°C to 96.84% at 55°C.

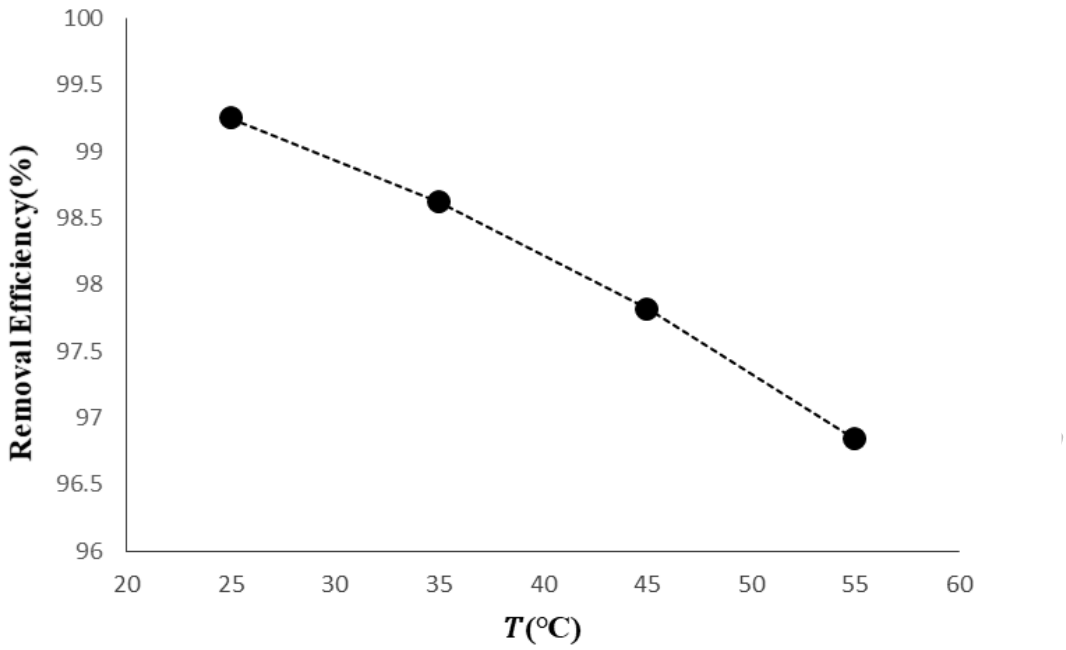

Fig. 10: The influence of temperature on the removal efficiency of lead ions by nZVI/NaY zeolite composite from aqueous solution

As the temperature rises, the adsorbed ions on the adsorbent surface gradually detach from the solid phase and re-enter the solution phase, resulting in a lower removal efficiency [62]. In other words, the electrostatic interactions weaken as the temperature increases, leading to a reduction in removal efficiency. The thermodynamic parameters are calculated using the subsequent equations:

$$\Delta G^{\circ} = -RT\ln(K_c) \quad (12)$$

$$\Delta G^{\circ} = \Delta H^{\circ} - T\Delta S^{\circ} \quad (13)$$

$$\ln(K_c) = -\left(\frac{\Delta H^{\circ}}{RT}\right) + \left(\frac{\Delta S^{\circ}}{R}\right) \quad (14)$$

$$K_c = \frac{\rho K_f}{1000}\left(\frac{10^6}{\rho}\right)^n \quad (15)$$

Where variation in Gibbs free energy (kJ/mol), entropy (kJ/mol.K), and enthalpy (kJ/mol) denoted by ΔG°, ΔS°, and ΔH° respectively, are considered. R (8.314 J/mol.K) and T denote the global constant of gases and the absolute temperature (K), respectively. We obtained the equilibrium constant K_C from the Freundlich constants (K_f and n), with ρ representing the density of pure water (~1.0 g/mL)) [68,69]. The ΔH° and ΔS° values were ascertained from the slope and intercept of the Van't Hoff plot of $\ln(K_C)$ against temperature. Table 6 presents all calculations.

Table. 6: Thermodynamic parameters for the lead ions adsorption by nZVI/NaY zeolite composite from aqueous solution

ΔS° (kJ/mol.K)	ΔH° (kJ/mol)	ΔG°(kJ/mol)	K_c	T (K)
-0.891	-367.2 70	-101.241	$5.58 * 10^{17}$	298
		-93.477	$7.14 * 10^{15}$	308
		-81.824	$2.76 * 10^{13}$	318
		-75.430	$1.03 * 10^{12}$	328

As observed, the ΔG° values are negative, demonstrating the spontaneity and feasibility of the adsorption process with the nZVI/NaY zeolite composite. As the temperature increases, the value of ΔG° rises from -101.241 to -75.430 kJ/mol, indicating a reduction in the degree of spontaneity of the reaction and causing the adsorption process to become more difficult. Based on ΔH° value, the adsorption process is exothermic. If the value falls within the range of -20 to -40 kJ/mol, the adsorption process can be considered physical, and if it falls within the range of -80 to -400 kJ/mol, it can be classified as chemical [70,71]. Accordingly, this value implies that the adsorption process is chemical. Additionally, a negative ΔS° value indicates reduced spontaneity at the adsorbate-solution interface [72].

Comparison of the adsorbent's performances

A comparative study was conducted to evaluate the effect of varying factors on adsorption, utilizing the nZVI/NaY zeolite composite in tandem with other reported adsorbents. Table 7 illustrates the findings, whereby a zeolite sourced from coal gangue demonstrated a maximum adsorption capacity of 482.1 and 431.6 mg/g at adsorbent dosages of 0.1 and 0.25 g/L, respectively, under conditions of initial concentration=200 mg/L, pH=7, and contact time=10 minutes. In a separate analysis, the zeolite-nZVI adsorbent demonstrated an adsorption capacity of 806 mg/g when tested at an initial concentration of 1000 mg/L. The adsorbent featured in this experiment possesses a substantial adsorption capacity and can remove substantial levels of lead from aqueous solutions. Of particular interest, the nZVI/NaY zeolite composite displays the highest adsorption capacity among all lead removal studies, with an exceptional adsorption capacity of 1652 mg/g at a concentration of 1000 mg/L. Furthermore, the Langmuir equation yielded a maximum adsorption capacity of 714.3 mg/g, which may bolster the strength of this study.

Table 7: Comparison of adsorption capacity for lead ions removal via various adsorbents.

Adsorbent	Pb (II) concentration (mg/L)	Adsorbent dosage (g/L)	pH	Time (min)	Adsorption capacity (mg/g)	References
Na-zeolite	15-300	2	4	60	66.96	[43]
MMZ	15-300	2	4	60	84	[43]
K-nZVI	500	5	5-6	60	440.5	[22]
Zeolite-nZVI	100-1000	1	4	140	99.2-806	[18]
NaY Zeolite (CG)	200	0.1, 0.25	7	10	482.1, 431.60	[57]
Mt–nZVI	200	2	5	40	100.53	[24]
Z–nZVI	200	2	5	40	85.44	[24]
Na-Y Zeolites (ZS)	1045–5890	20	4-4.5	120	299.6	[23]
Na-Y Zeolites (ZK)	1045–5890	20	4-4.5	120	299.3	[23]
Na-Y Zeolites (ZD)	1045–5890	20	4-4.5	120	260.6	[23]
Zeolite Y	100	0.2	6	60	454.5	[25]
CCSY (%5)	100	0.2	6	60	54.95	[25]
nZVI /NaY Zeolite	250	0.5	6	60	714.28	This work

Mechanism of adsorption

An equation based on the Weber-Morris theory was employed to study the mechanism governing lead adsorption at various adsorbent dosages. According to this theory, the adsorption capacity is intricately linked to the square root of time, as expressed by the equation:

$$q_t = K_{id}\, t^{0.5} + C \quad (16)$$

To better comprehend the manner in which lead particles adsorb to the active sites of the adsorbent, a q_t (mg/g) diagram was constructed versus $t^{0.5}$ ($min^{0.5}$). Notably, the results exhibited a consistent pattern across all three scenarios, as illustrated in Figure 11.

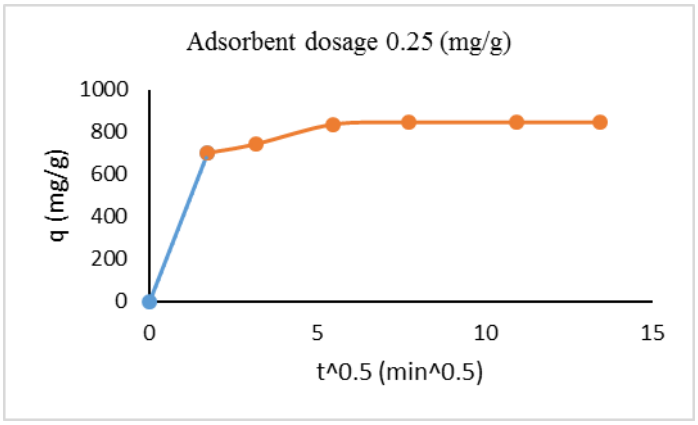

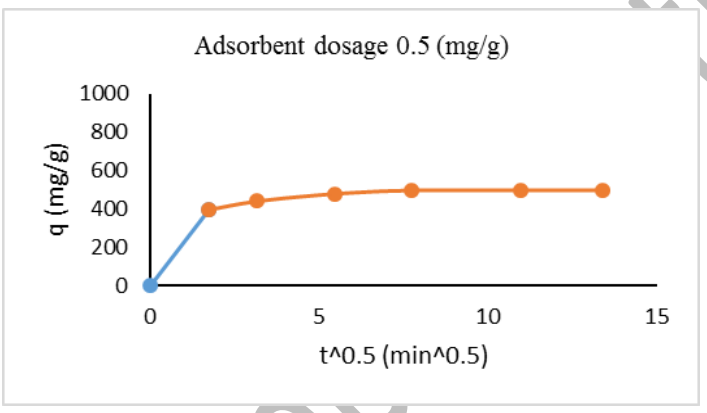

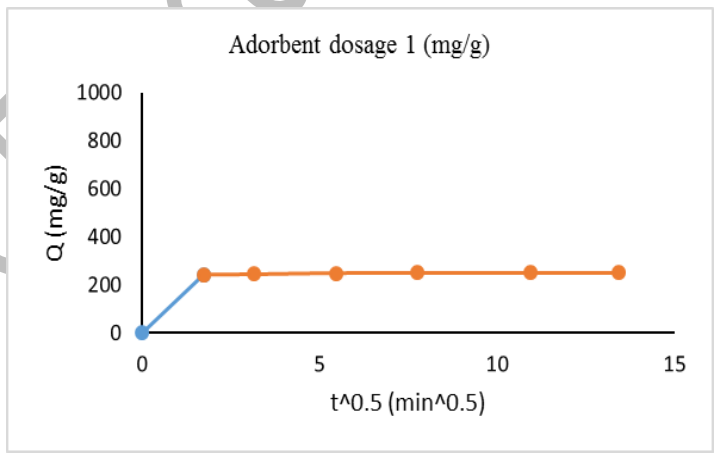

Fig. 11: Intraparticle diffusion diagrams

Each of the curves depicted in the diagrams exhibits a distinct duality characterized by two general segments. The initial segment, marked by a notably steeper slope, signifies substantial shifts in adsorption capacity over time. This rapid change is attributed to the pronounced concentration gradient acting as the driving force for adsorption between the adsorbent's surface and the surrounding bulk solution. In this initial phase, the trajectory of lead particles is from the bulk solution toward the adsorbent surface. Conversely, the subsequent segment, featuring a

gentler slope, reveals the prevalence of interparticle penetration, a naturally gradual phenomenon. In this latter phase, alterations in adsorption capacity occur more gradually as lead particles are adsorbed from the surface of the adsorbent into its internal pores. The nature of this process suggests a chemical adsorption mechanism, as corroborated by the kinetic data's closer alignment with the pseudo-second-order equation.

CONCLUSION

In this research, the NaY zeolite adsorbent in which functionalizing with zero-valent iron nanoparticles (nZVI/NaY zeolite) was successfully synthesized and the effective elimination of lead ions from water-based solutions have been investigated. The zero-valent iron nanoparticles were also well-entrapped with the zeolite matrix and then loaded over the surface of NaY zeolite. XRD and FESEM analyses proved that nZVI was correctly loaded and synthesized on the NaY zeolite support. The nZVI/NaY zeolite composite possessed a specific surface area measuring 418.6 m^2/g. The weight ratio of zero-valent iron nanoparticles to NaY zeolite was optimized at 1:4. The incorporation of zero-valent iron nanoparticles into NaY zeolite enhanced the removal efficiency and accelerated the adsorption process, enabling the removal of 99.25% of lead ions in 60 min. The kinetic data aligned well with the pseudo-second-order model, and the equilibrium data were well-suited to the Freundlich isotherm. Thermodynamic analysis indicated that the adsorption process was exothermic, spontaneous, and favorable. The mechanism of lead ion removal from aqueous solutions was identified as chemical adsorption. It is important to note that the synthesized adsorbent had a maximum adsorption capacity of 714.3 mg/g and a substantial adsorption capacity at an initial concentration of 1000 mg/L, which is equivalent to 1652 mg/g. The significance of the adsorption capacity in the nZVI/NaY zeolite adsorbent has been distinguished from other studies. Finally, it can be assumed that this adsorbent would be applied on an industrial scale. In addition, by the use of the magnetic properties in the iron nanoparticles, the separation at the end of the adsorption process might be feasible.

REFERENCES

[1] Raval, N. P., Shah, P. U. & Shah, N. K., Adsorptive Removal of Nickel (II) Ions From Aqueous Environment : A Review, *J. Environ. Manage.*, **179**: 1–20 (2016).

[2] Wang, S. *et al.*, Highly Adsorptive Pristine and Magnetic Biochars Prepared from Crayfish Shell for Removal of Cu (II) and Pb (II), *J. Taiwan Inst. Chem. Eng.*, **127**: 175–185 (2021).

[3] Santhosh, C. *et al.*, Role of Nanomaterials in Water Treatment Applications: A Review, *Chem. Eng. J.*, **306**: 1116–1137 (2016).

[4] Mardvar, A. *et al.*, Simultaneous Removal of Pb2+ And Cu2+ by SBA-15/Di-Urea as a Nano Adsorbent, *Iran. J. Chem. Chem. Eng.*, **41**: 163–173 (2022).

[5] Asuquo, E., Martin, A., Nzerem, P., Siperstein, F. & Fan, X., Adsorption of Cd(II) and Pb(II) Ions from Aqueous Solutions using Mesoporous Activated Carbon Adsorbent: Equilibrium, Kinetics and Characterisation Studies, *J. Environ. Chem. Eng.*, **5**: 679–698 (2017).

[6] Sajjadi, S. A. *et al.*, A Novel Route for Preparation of Chemically Activated Carbon from Pistachio Wood for Highly Efficient Pb(II) Sorption, *J. Environ. Manage.*, **236**: 34–44 (2019).

[7] Pandey, P. K., Sharma, S. K. & Sambi, S. S., Removal of Lead (II) from Waste Water on Zeolite-Nax, *J.*

Environ. Chem. Eng., **3**: 2604–2610 (2015).

[8] Jalu, R. G., Chamada, T. A. & Kasirajan, D. R., Calcium Oxide Nanoparticles Synthesis from Hen Eggshells for Removal of Lead (Pb(II)) from Aqueous Solution, *Environ. Challenges*, **4**: 100193 (2021).

[9] Fu, F. & Wang, Q., Removal of Heavy Metal Ions from Wastewaters: A Review, *J. Environ. Manage.*, **92**: 407–418 (2011).

[10] Duruibe, Ogwuegbu & Egwurugwu., Heavy Metal Pollution and Human Biotoxic Effects, *Int. J. Phys. Sci.*, **2**: 112–118 (2007).

[11] Ali, H., Khan, E. & Ilahi, I., Environmental Chemistry and Ecotoxicology of Hazardous Heavy Metals : Environmental Persistence , Toxicity , and Bioaccumulation, *Journal of chemistry*, **2019**: (2019).

[12] Jangkorn, S., Youngme, S. & Praipipat, P., Comparative Lead Adsorptions in Synthetic Wastewater by Synthesized Zeolite A of Recycled Industrial Wastes from Sugar Factory and Power Plant, *Heliyon* **8**: e09323 (2022).

[13] Pepe, F., de Gennaro, B., Aprea, P. & Caputo, D., Natural Zeolites for Heavy Metals Removal From Aqueous Solutions: Modeling of the Fixed Bed Ba2+/Na+ Ion-Exchange Process using a Mixed Phillipsite/Chabazite-Rich Tuff, *Chem. Eng. J.* **219**: 37–42 (2013).

[14] Sawant, S. Y., Pawar, R. R., Lee, S. M. & Cho, M. H., Binder-Free Production of 3D N-Doped Porous Carbon Cubes for Efficient Pb2+ Removal through Batch and Fixed Bed Adsorption, *J. Clean. Prod.*, **168**: 290–301 (2017).

[15] Rezania, S. *et al.*, Removal of Lead Ions from Wastewater using Lanthanum Sulfide Nanoparticle Decorated Over Magnetic Graphene Oxide, *Environ. Res.* **204**: 111959 (2022).

[16] Li, Y. *et al.*, Quantitatively Ion-Exchange between Mg (II) and Pb (II)/Cd (II) during the Highly Efficient Adsorption by Mgo-Loaded Lotus Stem Biochar, *J. Taiwan Inst. Chem. Eng.*, **144**: 104736 (2023).

[17] Iran Manesh, M., Sohrabi, M. R. & Mortazavi Nik, S., Nanoscale Zero-Valent Iron Supported on Graphene Novel Adsorbent for the Removal of Diazo Direct Red 81 from Aqueous Solution: Isotherm, Kinetics, and Thermodynamic Studies, *Iran. J. Chem. Chem. Eng.*, **41**: 1844–1855 (2022).

[18] Kim, S. A. *et al.*, Removal of Pb(II) From Aqueous Solution by a Zeolite-Nanoscale Zero-Valent Iron Composite, *Chem. Eng. J.*, **217**: 54–60 (2013).

[19] Azzam, A. M., El-Wakeel, S. T., Mostafa, B. B. & El-Shahat, M. F., Removal of Pb, Cd, Cu And Ni from Aqueous Solution using Nano Scale Zero Valent Iron Particles, *J. Environ. Chem. Eng.* **4**: 2196–2206 (2016).

[20] Oliveira, L. C. A., Petkowicz, D. I., Smaniotto, A. & Pergher, S. B. C. Magnetic Zeolites: A New Adsorbent For Removal Of Metallic Contaminants From Water, *Water Res.*, **38**: 3699–3704 (2004).

[21] Nguyen, C. H., Tran, M. L., Van Tran, T. T. & Juang, R.-S., Efficient Removal of Antibiotic Oxytetracycline from Water by Fenton-Like Reactions using Reduced Graphene Oxide-Supported

Bimetallic Pd/Nzvi Nanocomposites, *J. Taiwan Inst. Chem. Eng.*, **119**: 80–89 (2021).

[22] Zhang, X., Lin, S., Chen, Z., Megharaj, M. & Naidu, R., Kaolinite-Supported Nanoscale Zero-Valent Iron for Removal of Pb2+ From Aqueous Solution: Reactivity, Characterization and Mechanism, *Water Res.* **45**: 3481–3488 (2011).

[23] El-Mekkawi, D. M. & Selim, M. M., Removal of Pb2+ from Water by Using Na-Y Zeolites Prepared from Egyptian Kaolins Collected from Different Sources, *J. Environ. Chem. Eng.*, **2**: 723–730 (2014).

[24] Arancibia-Miranda, N. *et al.*, Nanoscale Zero Valent Supported by Zeolite and Montmorillonite: Template Effect of the Removal of Lead Ion From an Aqueous Solution, *J. Hazard. Mater.* **301**: 371–380 (2016).

[25] Shariatinia, Z. & Bagherpour, A., Synthesis of Zeolite Nay and its Nanocomposites with Chitosan as Adsorbents for Lead(II) Removal from Aqueous Solution, *Powder Technol.*, **338**: 744–763 (2018).

[26] Sun, Q. *et al.*, Subnanometric Hybrid Pd-M(OH)2, M = Ni, Co, Clusters in Zeolites as Highly Efficient Nanocatalysts for Hydrogen Generation, *Chem* **3**: 477–493 (2017).

[27] Ameri, A. *et al.*, Bio-Removal of Phenol by the Immobilized Laccase on the Fabricated Parent and Hierarchical Nay and ZSM-5 Zeolites, *J. Taiwan Inst. Chem. Eng.*, **120**: 300–312 (2021).

[28] Eljamal, O. *et al.*, Efficient Treatment of Ammonia-Nitrogen Contaminated Waters by Nano Zero-Valent Iron/Zeolite Composite, *Chemosphere* **287**: 131990 (2022).

[29] Zhang, X., Lin, S., Lu, X. Q. & Chen, Z. L., Removal of Pb(II) from Water using Synthesized Kaolin Supported Nanoscale Zero-Valent Iron, *Chem. Eng. J.*, **163**:243–248 (2010).

[30] Altamer, D. H., Alqazzaz, W. A. & Fadhi, A. B., Adsorption Behavior Of Rifampicin From Aqueous Solution Onto Locally Available Mud: Equilibrium, Kinetics, And Thermodynamic Study, *Iran. J. Chem. Chem. Eng. Res. Artic.*, **42**:139-154 (2023).

[31] Falyouna, O., Eljamal, O., Maamoun, I., Tahara, A. & Sugihara, Y., Magnetic Zeolite Synthesis for Efficient Removal of Cesium in a Lab-Scale Continuous Treatment System, *J. Colloid Interface Sci.*, **571**: 66–79 (2020).

[32] Beheshti, H., Irani, M., Hosseini, L., Rahimi, A. & Aliabadi, M., Removal of Cr (VI) from Aqueous Solutions using Chitosan/MWCNT/Fe3O4 Composite Nanofibers-Batch and Column Studies, *Chem. Eng. J.*, **284**: 557–564 (2016).

[33] Javidi, Z., Goudarzian, N., Mohammadi, M. K. & Tahanpesar, E., Synthesis and Drug Delivery Evaluation of Graphene Oxide Supported 5-Fluorouracil, *Iran. J. Chem. Chem. Eng.*, **42**: 1134–1146 (2023).

[34] Fatehi, M. H., Shayegan, J., Zabihi, M. & Goodarznia, I., Functionalized Magnetic Nanoparticles Supported On Activated Carbon For Adsorption Of Pb(II) And Cr(VI) Ions From Saline Solutions, *J. Environ. Chem. Eng.*, **5**: 1754–1762 (2017).

[35] Araújo, C. S. T. *et al.*, Elucidation of Mechanism Involved in Adsorption of Pb(II) onto Lobeira Fruit (Solanum Lycocarpum) using Langmuir, Freundlich and Temkin Isotherms, *Microchem. J.*, **137**:348–354

(2018).

[36] Teoh, Y. P., Khan, M. A. & Choong, T. S. Y., Kinetic and Isotherm Studies for Lead Adsorption from Aqueous Phase on Carbon Coated Monolith, *Chem. Eng. J.*, **217**: 248–255 (2013).

[37] Saravaia, H., Ray, S., Chanchpara, A. & Bhatt, D., Preparation Of Surface Amino Modified Magnesium Doped Lithium Manganese Oxide Nanosorbent And Its Investigation For Dye Removal, *Iran. J. Chem. Chem., Eng. Res. Artic.*, **42**: 3069-3078 (2023).

[38] Merad Boudia, S., Benabadji, K. I. & Bouras, B., Adsorption of Anionic Dye from Aqueous Solution using Activated Montmorillonite/Graphene Oxide/Gelatin Composites, *Iran. J. Chem. Chem. Eng. Res. Artic.*, **42**: 1527-1537 (2023).

[39] Mohamed, F. *et al.*, Activated Carbon Derived From Sugarcane And Modified With Natural Zeolite For Efficient Adsorption Of Methylene Blue Dye : Experimentally And Theoretically Approaches, *Sci. Rep.*, **12**: 1–18 (2022).

[40] Adebisi, G. A., Chowdhury, Z. Z. & Alaba, P. A., Equilibrium, Kinetic, and Thermodynamic Studies of Lead Ion and Zinc Ion Adsorption from Aqueous Solution onto Activated Carbon Prepared From Palm Oil Mill Effluent, *J. Clean. Prod.*, **148**: 958–968 (2017).

[41] Siu, P. C. C., Koong, L. F., Saleem, J., Barford, J. & McKay, G., Equilibrium and Kinetics of Copper Ions Removal from Wastewater by Ion Exchange, *Chinese J. Chem. Eng.*, **24**: 94–100 (2016).

[42] Karthik, R. & Meenakshi, S., Removal of Pb(II) and Cd(II) Ions from Aqueous Solution using Polyaniline Grafted Chitosan, *Chem. Eng. J.* **263**: 168–177 (2015).

[43] Yuan, M., Xie, T., Yan, G., Chen, Q. & Wang, L., Effective Removal of Pb2+ from Aqueous Solutions by Magnetically Modified Zeolite, *Powder Technol.*, **332**: 234–241 (2018).

[44] de Oliveira, L. H. *et al.*, H2S Adsorption on Nay Zeolite, *Microporous Mesoporous Mater.*, **284**: 247–257 (2019).

[45] Oruji, S., Khoshbin, R. & Karimzadeh, R., Preparation of Hierarchical Structure of Y Zeolite with Ultrasonic-Assisted Alkaline Treatment Method used in Catalytic Cracking of Middle Distillate Cut: The Effect Of Irradiation Time, *Fuel Process. Technol.*, **176**: 283–295 (2018).

[46] Xue, M. *et al.*, Selective Adsorption of Thiophene and 1-Benzothiophene on Metal-Ion-Exchanged Zeolites in Organic Medium, *J. Colloid Interface Sci.*, **285**: 487–492 (2005).

[47] Zhou, S. *et al.*, Enhanced Cr(Vi) Removal from Aqueous Solutions using Ni/Fe Bimetallic Nanoparticles: Characterization, Kinetics and Mechanism, *RSC Adv.* **4**: 50699–50707 (2014).

[48] Ríos R, C. A., Oviedo V, J. A., Henao M, J. A. & Macías L, M. A., A Nay Zeolite Synthesized from Colombian Industrial Coal By-Products: Potential Catalytic Applications, *Catal. today*, **190**: 61–67 (2012).

[49] Üzüm, Ç. *et al.*, Synthesis and Characterization of Kaolinite-Supported Zero-Valent Iron Nanoparticles

and their Application for the Removal of Aqueous Cu2+ And Co2+ Ions, *Appl. Clay Sci.*, **43**: 172–181 (2009).

[50] Liu, Y., Phenrat, T. & Lowry, G. V., Effect of Tce Concentration and Dissolved Groundwater Solutes on Nzvi-Promoted Tce Dechlorination and H2 Evolution, *Environ. Sci. Technol.*, **41**: 7881–7887 (2007).

[51] Zeng, Y., Walker, H. & Zhu, Q. Reduction of Nitrate by Nay Zeolite Supported Fe, Cu/Fe and Mn/Fe Nanoparticles, *J. Hazard. Mater.*, **324**: 605–616 (2017).

[52] Zhou, C., Han, C., Min, X. & Yang, T., Simultaneous Adsorption of As (V) And Cr (VI) by Zeolite Supporting Sulfide Nanoscale Zero-Valent Iron: Competitive Reaction, Affinity and Removal Mechanism, *J. Mol. Liq.*, **338**: 116619 (2021).

[53] Deng, C. *et al.*, The Effect Of Positioning Cations on Acidity and Stability of the Framework Structure of Y Zeolite, *Sci. Rep.*, **6**: 23382 (2016).

[54] Wang, Q., Song, X., Tang, S. & Yu, L., Enhanced Removal of Tetrachloroethylene from Aqueous Solutions by Biodegradation Coupled with nzvi Modified by Layered Double Hydroxide, *Chemosphere* **243**: 125260 (2020).

[55] He, X. *et al.*, Effects of Coal Pore Structure on Methane- Coal Sorption Hysteresis: An Experimental Investigation Based on Fractal Analysis and Hysteresis Evaluation, *Fuel*, **269**: 117438 (2020).

[56] Li, S., Yang, F., Zhang, Y., Lan, Y. & Cheng, K., Performance of Lead Ion Removal by the Three-Dimensional Carbon foam Supported Nanoscale Zero-Valent Iron Composite, *J. Clean. Prod.*, **294**: 125350 (2021).

[57] Bu, N. *et al.*, Synthesis of Nay Zeolite from Coal Gangue And its Characterization for Lead Removal from Aqueous Solution, *Adv. Powder Technol.*, **31**: 2699–2710 (2020).

[58] Wang, W., Zhou, M., Mao, Q., Yue, J. & Wang, X., Novel Nay Zeolite-Supported Nanoscale Zero-Valent Iron As an Efficient Heterogeneous Fenton Catalyst, *Catal. Commun.*, **11**: 937–941 (2010).

[59] Zhang, Y. Y., Jiang, H., Zhang, Y. & Xie, J. F., The Dispersity-Dependent Interaction Between Montmorillonite Supported nZVI and Cr(VI) in Aqueous Solution, *Chem. Eng. J.*, **229**: 412–419 (2013).

[60] Bhowmick, S. *et al.*, Montmorillonite-Supported Nanoscale Zero-Valent Iron for Removal of Arsenic From Aqueous Solution: Kinetics and Mechanism, *Chem. Eng. J.*, **243**: 14–23 (2014).

[61] Arshadi, M., Soleymanzadeh, M., Salvacion, J. W. L. & SalimiVahid, F., Nanoscale Zero-Valent Iron (NZVI) Supported on Sineguelas Waste for Pb (II) Removal from Aqueous Solution: Kinetics, Thermodynamic and mechanism, *J. Colloid Interface Sci.*, **426**: 241–251 (2014).

[62] Ghahremani, A., Manteghian, M. & Kazemzadeh, H., Removing Lead From Aqueous Solution By Activated Carbon Nanoparticle Impregnated On Lightweight Expanded Clay Aggregate, *J. Environ. Chem. Eng.* **9**: 104478 (2021).

[63] Krishnamoorthy, R. *et al.*, Date Pits Activated Carbon For Divalent Lead Ions Removal, *J. Biosci. Bioeng.*

128: 88–97 (2019).

[64] Sing, K. S. W., Reporting Physisorption Data for Gas/Solid Systems with Special Reference to The Determination of Surface Area and Porosity (Recommendations 1984). *Pure Appl. Chem.* **57**: 603–619 (1985).

[65] Nieto-Márquez, A., Pinedo-Flores, A., Picasso, G., Atanes, E. & Sun Kou, R., Selective Adsorption of Pb2+, Cr3+ and Cd2+ Mixtures on Activated Carbons Prepared from Waste Tires, *J. Environ. Chem. Eng.* **5**: 1060–1067 (2017).

[66] Mahmoud, M. E., Saad, E. A., Soliman, M. A. & Abdelwahab, M. S., Removal of Radioactive Cobalt/Zinc And Some Heavy Metals from Water using Diethylenetriamine/2-Pyridinecarboxaldehyde Supported on NZVI, *Microchem. J.*, **145**: 1102–1111 (2019).

[67] Campos, A. F. C. *et al.*, Core-Shell Bimagnetic Nanoadsorbents for Hexavalent Chromium Removal from Aqueous Solutions, *J. Hazard. Mater.*, **362**: 82–91 (2019).

[68] Lima, R. R. C., De Lima, P. D. S., Greati, V. R., De Sousa, P. B. F. & Medeiros, G. V. S., Sodium-Modified Vermiculite For Calcium Ion Removal From Aqueous Solution, *Ind. Eng. Chem. Res.*, **58**: 9380–9389 (2019).

[69] Tong, Y., Mayer, B. K. & McNamara, P. J., Adsorption of Organic Micropollutants to Biosolids-Derived Biochar: Estimation of Thermodynamic Parameters, *Environ. Sci. Water Res. Technol.*, **5**: 1132–1144 (2019).

[70] Nagarajan Vijayanand; Ganesan, Raja ,Govindaraj, P., Hybrid Cross-Linked Bio Polymer-Epichlorohydrin / Fe 3 O 4 Nanocomposite for As (V) Adsorption : Kinetic , Isotherm , Thermodynamic , and Mechanism Study, *Iran. J. Chem.*, **41**: 3319–3333 (2022).

[71] Barmaki, Z., Aghaie, H., Seif, A. & Monajjemi, M., Kinetic and Thermodynamic Study of Chromium Picolinate Removing from Aqueous Solution onto the Functionalized Multi-Walled Carbon Nano Tubes, *Iran. J. Chem. Chem. Eng.*, **40**: 765–779 (2021).

[72] Aiyesanmi, A. F., Adebayo, M. A., Okoronkwo, A. E. & Ekujumi, O., Adsorption of Nickel (II) from Aqueous Solution using Leucaena Leucocephala Shells, *Iran. J. Chem. Chem. Eng. Res. Artic.*, **41**: (2022).